Magazine of Civil Engineering

ISSN 2712-8172

journal homepage: http://engstroy.spbstu.ru/

Research article

UDC 624.03

DOI: 10.34910/MCE.133.3

Dynamic behavior of a reinforced concrete slab of a pedestrian bridge with stiff rebars

A.V. Alekseytsev[1] ✉, ***K.V. Kvocak***[2], ***D.S. Popov***[1], ***M. Al Ali***[2]

[1] *Moscow State University of Civil Engineering (National Research University), Moscow, Russian Federation*

[2] *Technical University in Košice, Košice, Slovak Republic*

✉ *aalexw@mail.ru*

Keywords: dynamics, rigid reinforcement, accidental failure, numerical modelling, reinforced concrete slabs, mechanical impact

Abstract. Evaluation of the ultimate bearing capacity of a reinforced concrete slab of a pedestrian bridge with stiff rebars is a relevant issue investigated in the article. Dynamic analysis takes account of low velocities of dynamic loading. A 3D model of a structure is made. A stiff rebar is a U-shaped perforated profile welded to the plate. The focus of the computation methodology is the model verification. Towards this end, mechanical characteristics of materials are experimentally identified; full-size specimens are made and subjected to static load testing. The numerical study focuses on analyzing two sessions of loading by an impactor located in the center of a span. The impactor has symmetrical and nonsymmetrical impact spots. Dynamic loading is proposed to be simulated in several stages. At the final stage, the structure vibrates together with the impactor. The Menétrey–Willam model is chosen to describe the deformation of concrete; the stress-strain state of the structure and stiff rebars is described by a curvilinear diagram that conveys strengthening and shows the actual behavior of the rebars. An implicit integration scheme is employed to identify detailed dependences showing the time-dependent change in the stress-strain state components affecting structural safety. The conclusion is that nonsymmetrical loading is the most substantial dynamic effect, and stiff rebars can greatly increase the survivability of the system subjected to impacts of man-induced origin.

Citation: Alekseytsev, A.V., Kvocak, K.V., Popov, D.S., Al Ali, M. Dynamic behavior of a reinforced concrete slab of a pedestrian bridge with stiff rebars. Magazine of Civil Engineering. 2025. 18(1). Article no. 13303. DOI: 10.34910/MCE.133.3

1. Introduction

The present-day socio-economic environment triggers the need to design structures of infrastructure, including elements of engineering structures featuring higher mechanical safety. Safety assurance is vital if a structure is subjected to various man-induced effects such as mechanical impacts, explosions, fires, etc. Concrete, reinforced concrete, steel fiber reinforced concrete and other composite structures are often subjected to such effects [1–5]. The dynamic behavior of load-bearing structures is investigated as a function of the rate of application of dynamic load. In some cases when the dynamics of low velocities is addressed [6, 7], the load is represented as pulses of various forms varying in time. If high velocity dynamics is considered [8–10], dynamic load is applied explicitly, and explicit solvers are used to make the finite element analysis of the problem. The von Mises stress is the fracture criterion for elements made of structural steel; principal stresses, calculated using well-known models of Menétrey–Willam, Drucker–Prager, etc., are the fracture criteria for concrete.

Bridges and bridge structures, subjected to mechanical impacts, are investigated. A computational tool, designed for low-speed dynamics, is employed to analyze various impacts, including those impacts that are triggered by the movement of high-speed trains [11], collisions with heavy machinery [12], impact interaction with ships and barges [13, 14], as well as impacts from rock falling on bridges in mountainous areas [15, 16]. Pedestrian bridges and their structural components can also be subjected to similar impacts. Impacts from a falling body can be effectively analyzed using technologies developed for modeling emergency effects on buildings and structures. First of all, these are the approaches related to elements of pull-down analysis [17–22] and methods of direct integration using implicit integration schemes [23–25].

In most cases, an increase in the safety of structures subjected to dynamic loading means an increase in the consumption of materials or a higher damping capacity of a system. Relevant analytical studies show that such an effect can be achieved by the targeted regulation of natural vibration frequencies of a structure that requires special connections or a change in the stiffness of individual elements of a system [26, 27]. However, such approaches are implemented only for the simplest beam systems made of isotropic materials. Therefore, numerical simulation is the main tool for analyzing the rationality of design solutions.

The modeling of loads, reproducing dynamic impacts on a structure, is also an important and relevant problem [28–32]. When low impact velocities are considered, two techniques can be used: the first one is pulse loading and the second one is a combination of the lumped mass attached to a GAP element, in which the gap value determines the height of the load fall for the case where free falling has gravitational acceleration.

Damping is the key determinant of dynamic analysis results. Dynamic analysis can encompass physical attenuation models and numerical damping used to stabilize the iterative process of computations. Physical attenuation models encompass a well-known Rayleigh scheme, in which a stiffness matrix is used to take into account internal friction forces, and a mass matrix is used to take into account resistance of the medium. The V.N. Sidorov model [33] and the Kelvin–Voigt model are no less effective.

This paper addresses numerical modeling of a pedestrian bridge slab subjected to symmetrical and nonsymmetrical dynamic effects. Pulse load is described by the shape of a complex polygon, reproducing the transfer of kinetic energy of an impactor and subsequent joint oscillation of the system. The ultimate dynamic load is determined. The danger of symmetrical and nonsymmetrical dynamic effects, the nature of fracture, and the ability of stiff reinforcement to take load are identified.

The objective of the work is to evaluate the mechanical safety of slabs used for pedestrian bridge spans under dynamic effects. In order to achieve this goal, the following main tasks were solved:

- creation of the structural solution with the use of rigid reinforcement for the slab structure in the form of metal profiles (stiff rebars);
- experimental study of the slab with stiff rebars, during which the mechanical properties of the materials and the ultimate loads were determined, allowing the design model to be verified;
- numerical modelling of the deformations of the structure under symmetrical and asymmetrical dynamic actions, using the characteristics of the materials and the dimensions of the experimental specimens.

2. Methods and Materials

2.1. Subject of Research and Problem Statement

The purpose of the study is to evaluate the stress-strain state and ultimate load for pedestrian bridge slabs with stiff rebars in the case of dynamic loading. The following research program was implemented to achieve this purpose:

- production of a pedestrian bridge slab and experimental determination of the ultimate static load;
- verification of the finite element model of the subject of research under static loading;
- development of a numerical model of a structure under dynamic loading and its analysis.

The study focuses on the deformation of a slab subjected to symmetrical and nonsymmetrical dynamic loading that can trigger its ultimate state.

The subject of the study is a steel reinforced concrete slab of a pedestrian bridge with a metal profile installed in the tensile zone (Fig. 1a, b). The length of the slab is 6000 mm (the distance between the bridge supports is 5800 mm); the bridge width is 900 mm; the bridge height is 270 mm. The slab has conventional and stiff rebars; they are two steel metal profiles, each has two parts. The bottom part is a solid metal sheet; its thickness is 9.2 mm, and the top part is 8.0 mm thick. It is U-shaped (rotated through an angle of 180

degrees). The lateral surface of profiles has openings with a diameter of 50 mm; they are spaced at intervals of 100 mm. The top and bottom zones of the slab have structural rebars with a diameter of 14 mm.

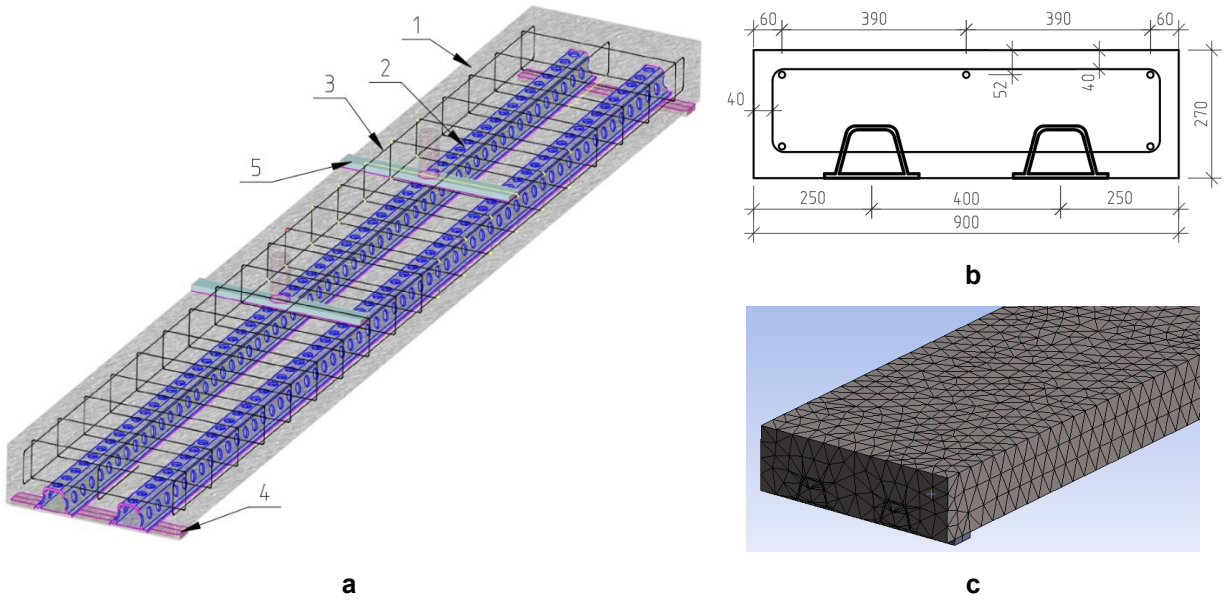

a b c

Figure 1. The subject of the study: (a) general view of a pedestrian slab: 1 – concrete, 2 – stiff rebars; 3 – flexible structural rebars, 4 – structure of supports, 5 – point of load transfer; (b) standard cross-section of the slab; (c) finite element model of a slab.

2.2. Numerical Model of the Structure

2.2.1. Description of the finite element model

Ansys software package was used for numerical modeling purposes. Decomposition of the solid body, describing concrete for this model, involves some difficulty due to the presence of stiff rebars in the slab. Attempts to generate a good quality element mesh, using only rectangular 8-node finite elements, were not successful. Therefore, the mesh was generated automatically (Fig. 1c). The size of the finite element was 50 mm. Modeling of stiff rebars and concrete was performed using Solid 186 (20-node finite element) and Solid 187 (10-node tetrahedral finite element).

2.2.2. Models of materials

The behavior of concrete was described using the Menétrey–Willam model [34]. As a rule, the Menétrey–Willam model is better at modeling the behavior of binding aggregates, such as concrete than, for example, the Drucker–Prager model without supplementary modifications [35, 36]. This model is based on the theory of plastic flow.

The model of concrete has three main components:

1. A three-invariant limit surface f_{MW} (Fig. 2), described by equation (1), where s_2 and s_3 are the equation parameters, controlling the shape of the meridional cross-section of the surface and determined from yield strengths in uniaxial tension $\left(R_t\right)$, compression $\left(R_c\right)$ and biaxial compression $\left(R_b\right)$ [37, 38]. The limit surface conveys the strength condition of the material in the Haig–Westergaard principal stress space. This surface has a single singularity point located at the vertex, in the neighborhood of triaxial tension.

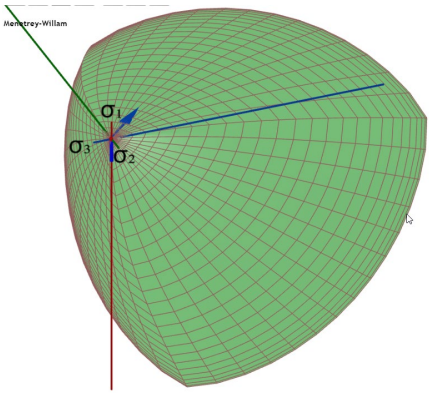

$$f_{MW} = \frac{c_2}{c_3}\left[\sqrt{2\xi} + rp\right] + p^2 - \frac{1}{c_3}; \quad (1)$$

$$Q_{MW} = \rho^2 + B_g p + C_g \xi; \quad (2)$$

$$B_g = \frac{2 \cdot \left(\sqrt{2} \cdot \tan\left(\Psi_b\right) \cdot R_b - R_{bt}\right)}{\sqrt{3}\left(1/\sqrt{2} - \tan\left(\Psi_b\right)\right)}; \quad (3)$$

$$C_g = \frac{B_g}{\sqrt{2}} + 2 \cdot \frac{R_{bt}}{\sqrt{3}}. \quad (4)$$

Figure 2. Limit surface of the Menétrey–Willam model and basic expressions used to describe it.

2. Plastic potential surface [35], responsible for the direction of the vector of plastic deformations, described by equations (2)–(4), where Ψ_b is the dilatation angle of concrete in uniaxial compression, which is the quotient of the tensor norm of plastic 3D deformations divided by the deviator norm of plastic deformations; B_g and C_g are parameters characterizing the plastic potential. Values of the dilatation angle, depending on the class of concrete, can be taken from Table 1 [37].

Table 1. Dependence of the dilatation angle on the class of concrete.

Concrete class	B15	B20	B25	B30	B35	B40	B45	B50
ψ_b	4.59	5.68	6.62	7.42	8.24	9.17	9.98	11.13

3. Laws of the limit surface evolution, responsible for strengthening and softening of the material. The model separately conveys evolution laws for compression (see Fig. 3a) and tension (see Fig. 3b).

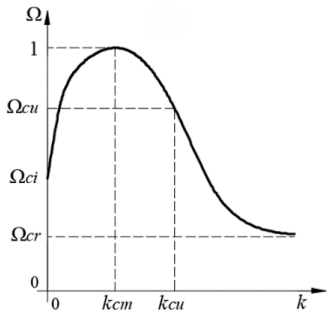

a

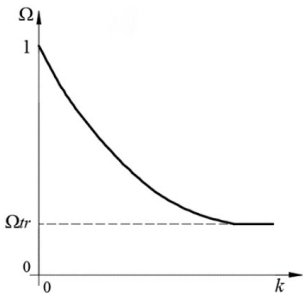

b

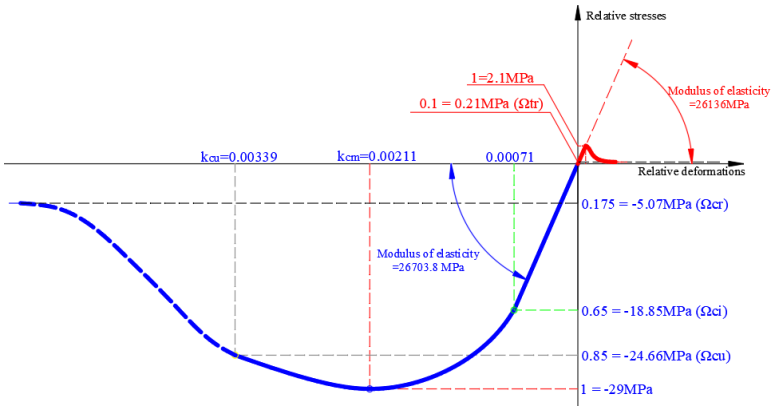

c

Figure 3. Absolute and relative stress-strain curves.

Exponential softening in compression and tension is used to describe the behavior of concrete in the process of softening. Values of standard stresses and plastic strains at characteristic points are employed for this purpose. Elastic strains, obtained for relative stress $\Omega = 0.65,$ are subtracted from total strains, obtained for relative stresses $\Omega = 1.0$ and $\Omega = 0.85.$ These elastic strains can be computed according to recommendations provided in applicable regulations, such as Construction Regulations 63.13330.2018. Fig. 3c shows the concrete diagram used in the analysis of a pedestrian bridge slab.

Concrete fracture was taken into account in the analysis. Fracture energy G_F is the parameter characterizing the softening of material under tension [39]. This parameter conveys the amount of energy that must be transmitted to the material to stop the transmission of stresses between the crack edges (to completely break the atomic bonds). Graphically, this value corresponds to the Gft area in Fig. 4. The deformation of stiff rebars was described by a multilinear dependence accompanied by hardening (Fig. 5). Values of strains in the diagrams, conveying the behavior of steel and concrete, are assumed to be plastic in Ansys. The elastic behavior is identified using the value of the modulus of elasticity.

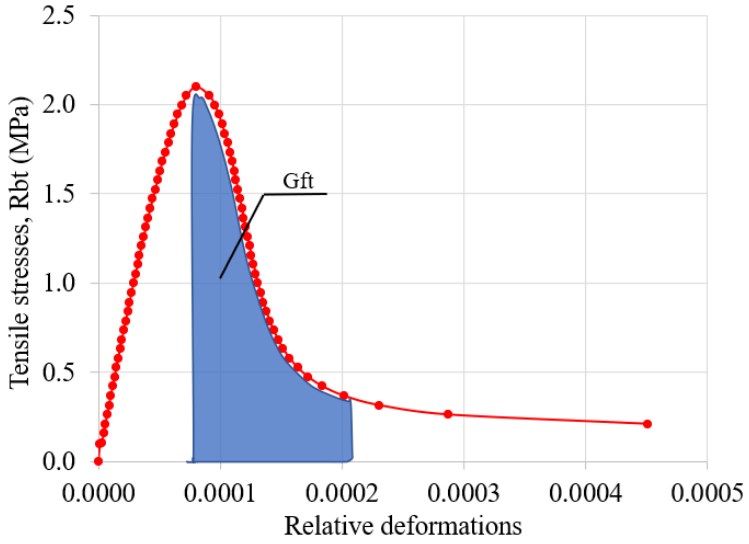

Figure 4. Fracture energy G_F and the tensile curve of concrete.

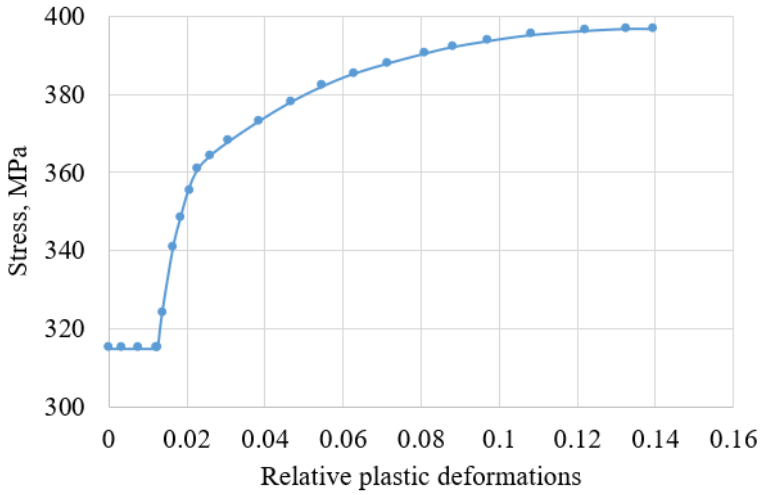

Figure 5. Multilinear diagram of stiff rebar deformation.

Strength characteristics of concrete and steel, used in the numerical computation, were identified in the course of an experimental study [40]. Structural slab reinforcement, made using individual (flexible) bars, was simulated by discrete 3D finite elements REINF264. Hence, there was no need to decompose the finite element mesh in such a way that rebar elements were connected to nodes of 3D elements (simulating concrete). Therefore, a better mesh can be obtained for the models [41, 42]. The behavior of conventional reinforcement steel is described by the bilinear relationship at the yield strength of 400 MPa.

2.2.3. Slab loading and support constraints

The bridge slab model was calculated for the case of the load application to two different zones (Fig. 6), which correspond to the most dangerous points of loading.

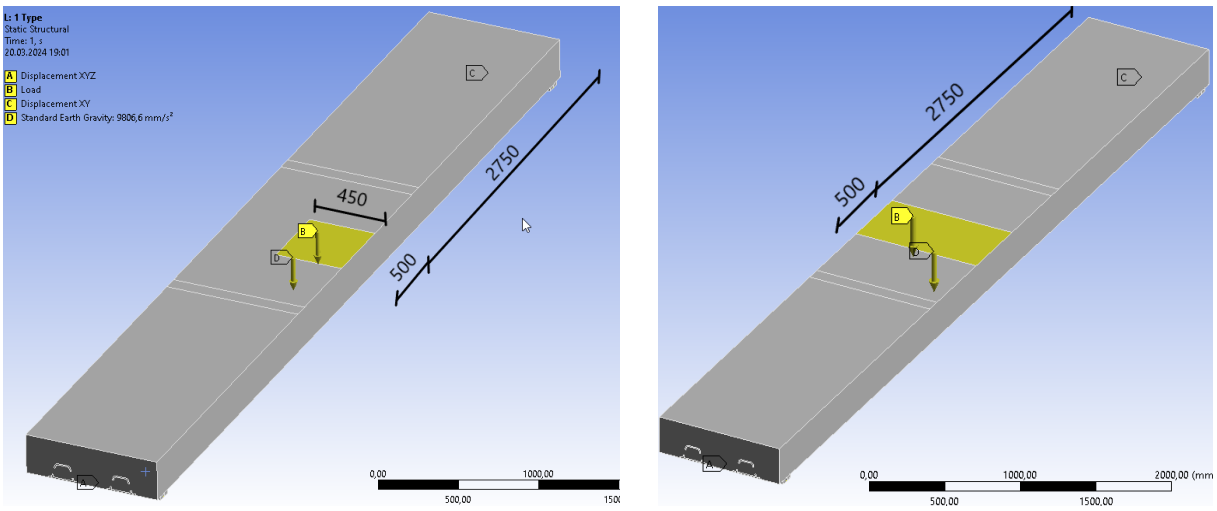

a b

Figure 6. Nonsymmetrical (a) and symmetrical (b) floor slab loading.

The general idea of dynamic load application (Fig. 7a) is as follows:

– application of dead load and stabilization of vibrations (the first stage);
– pulse load increase that simulates the accelerated fall of bodies on the bridge; free fall or other man-induced impact (the second stage);
– maximum pulse value for some period of time (the third stage);
– drop in the pulse load and vibration of the structure together with the impactor (the fourth stage).

Without considering the details of the impact load computation, the maximum value of the pulse load was determined as 90 % of the ultimate value under static loading (determined in the first computation step).

In terms of time, the load was applied to the floor slab in four stages (Fig. 12). Fig. 12 shows the coefficients, by which the load constant is multiplied, meaning that the maximum value of the load is equal to unity in the graph.

The first stage, or the application of dead load, takes 0.5 sec; the second stage, or an increase in dynamic load, takes 0.2 sec; the third stage, or the stabilization of load at the peak value, takes 0.5 sec; the fourth stage, or a reduction in dynamic load to 10 % of the peak value, takes 0.2 sec.

Support components are simulated by separate elements, which are in turn decomposed into two parts: a panel and a line. The panel is hinge-fixed to the slab, and line A has a sliding hinge connection to the panel (Fig. 7b). This way of modeling the boundary conditions better conveys the realistic behavior of supports connected to the slab. It does not trigger any supplementary forces in the support zone and allows for the rotation, preventing the support bending moment.

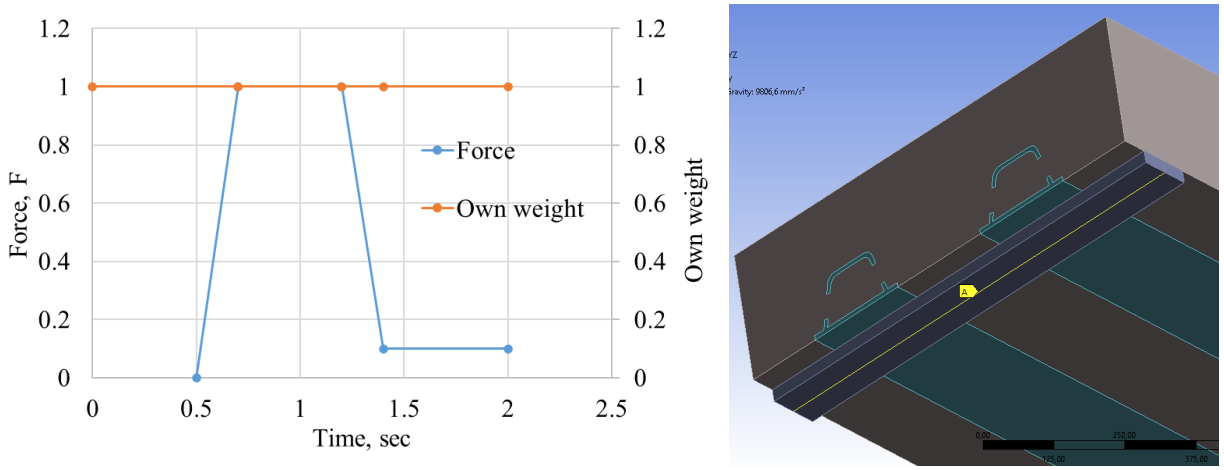

a b

Figure 7. Loading history (a); slab support (b).

2.2.4. Description of the finite element solver

Initially, computations are performed in the Ansys Static Structural module to evaluate the load-bearing capacity of the slab under static loading. At the second stage, modal analysis (Modal analysis module) is performed to find natural frequencies of vibration required to determine the damping properties of the system. At the final stage needed to solve the problem of structural dynamics, the computation is performed in the Transient Structural module, which is based on implicit schemes of integration of the equation of motion, taking into account inertial and damping forces. An important positive property of the Transient Structural module is that this module can be used together with the Static Structural model, meaning that the geometry and all parameters of the material (concrete, rebars, concrete reinforcement, etc.) can be used in computations without changes, except for setting the parameters of dynamic analysis.

The equation of motion used to analyze the dynamic response of structures [34]:

$$F(t)=[M]\{u\}''+[C]\{u\}'+[K]\{u\}, \tag{1}$$

where $[M]$ is the mass matrix; $[C]$ is the damping matrix; $[K]$ is the stiffness matrix; $F(t)$ is the load; $\{u\}''$ is the nodal acceleration vector; $\{u\}'$ is the nodal velocity vector; $\{u\}$ is the node displacement vector.

At any point in time, these equations can be represented as a set of "static" equilibrium equations that also take into account forces of inertia $([M]\{u\}')$ and forces of damping $\left([C]\{u\}'\right)$. The Transient Structural module uses the Newmark time integration method to solve equations at discrete points in time. Damping is one of the main computation parameters for dynamic loading. Two types of damping, numerical and physical damping, are available in the Ansys software package.

Numerical (artificial) damping is necessary to stabilize problem solving. There are several types of settings for the Newmark α and β parameter method that use the same system of equations:

$$\delta=\frac{1}{2}+\gamma;\ \alpha=\frac{1}{4}(1+\gamma)^2, \tag{2}$$

where γ is the value of numerical damping.

The value of numerical damping is constant depending on the selected type of solver setting, namely: Impact $-\gamma=0$; High speed dynamics $-\gamma=0.005$; Moderate speed dynamics $-\gamma=0.1$; Low speed dynamics $-\gamma=0.414$.

Rayleigh constants α and β were used to take into account physical damping. These constants, multiplied by the mass matrix $[M]$ and the stiffness matrix $[K]$, are used to compute the damping matrix $[C]$:

$$[C]=\alpha[M]+\beta[K]. \tag{3}$$

In Ansys, two approaches, including "Direct input" and "Damping vs Frequency", can be used to take into account physical damping. In the first approach, Rayleigh alpha and beta coefficients are input directly, meaning that they have specific values. In this computation, the second approach is used, where the natural frequency of vibration (ω) is applied; the damping coefficient (ξ) equals 0.05 for reinforced concrete; the alpha coefficient equals zero (given that the external environment has no effect), and the beta coefficient is automatically determined in the solver using the formula:

$$\beta=\frac{2\xi}{\omega}. \tag{4}$$

The frequency of natural vibrations of the bridge slab was determined in the module "Modal analysis", and it equals 14.3 Hz.

2.3. *Experimental Verification of the Numerical Model of the Structure*

Computations were made to verify the results obtained using the numerical model. The conditions and characteristics of these computations corresponded to the experimental tests described in detail in [40]. The computation model had the following characteristics of materials obtained during the test: cylinder strength of concrete – 32.17 MPa; yield strength and ultimate tensile strength of stiff steel rebars – 315 MPa and 396 MPa, respectively; yield strength of flexible rebars – 355 MPa.

Fig. 8 shows the graphical dependence between slab deflection and load in the experimental specimen and numerical model.

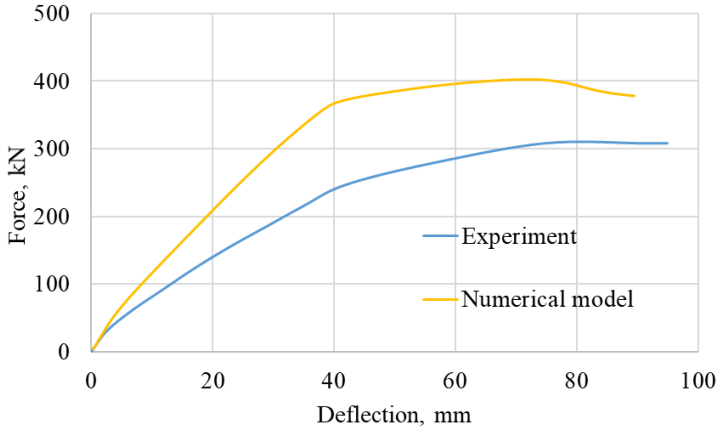

Figure 8. Dependence between deflection and load in experimental and numerical models.

The comparative analysis of (1) load-deflection dependencies for experimental specimens and (2) the results of numerical computation are in good agreement. The discrepancy between deflection values is 3 %; the discrepancy between values of the fracture force does not exceed 24 %. It confirms the proper modeling of strength and stiffness characteristics of materials, types of finite elements, boundary conditions, models simulating the behavior of concrete and rebars, and, as a result, it allows for reliable numerical studies of these models by changing the type and area of application of loads. The general view of experimental specimens and the course of the experiment is shown in Fig. 9.

a

b

c d

Figure 9. Experimental testing of the pedestrian bridge slab: general view of the testing bench (a), load application scheme (b), reinforcement frame (c), testing the cube and cylinder strength of concrete specimens (d).

The compressive strength of the concrete specimens (Fig. 9d) and the tensile strength of the rebars were experimentally determined earlier. Then pedestrian slab specimens were fabricated. Their reinforcement scheme is shown in Fig. 9c. Slab specimens were mounted on a steel frame (Fig. 9a) and subjected to ultimate static loading using two power generation units (Fig. 9b). Experimentally determined mechanical characteristics of materials and average measured values of 3D dimensions of the specimen were used in the computations.

3. *Results and Discussion*

The ultimate load and deflections under symmetrical and nonsymmetrical loading are determined from the results of numerical computations of models subjected to static and dynamic loading. Under nonsymmetrical loading, the maximum static ultimate load and deflection values are 318.3 kN and 55.8 mm; under dynamic loading, they equal 345.2 kN and 53.41 mm. Under symmetrical loading, the maximum static ultimate load and deflection values are 291.1 kN and 52.1 mm; under dynamic loading – 331.7 kN and 42.8 mm.

Figs. 10a, 10b show the ultimate static load under symmetrical and nonsymmetrical loading. Figs. 10c, 10d show a time change in deflection (f-c) and actual load (N-c). On average, the ultimate value of deflection under nonsymmetrical loading was 30 % higher than under symmetrical loading, and the discrepancy between values of ultimate dynamic load did not exceed 10 %, which translates into a greater danger of nonsymmetrical emergency effects for such structures.

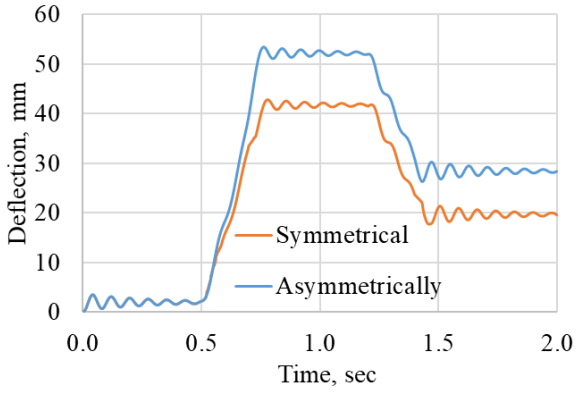

a

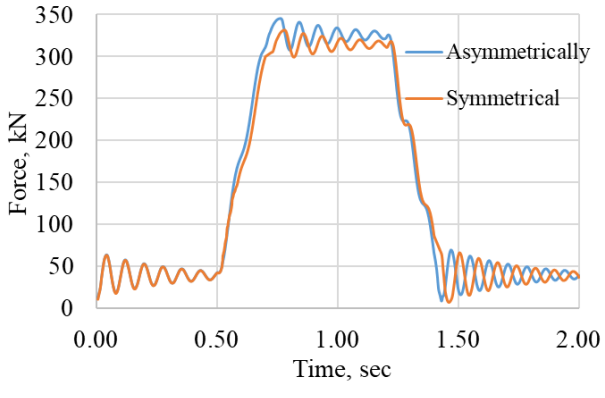

b

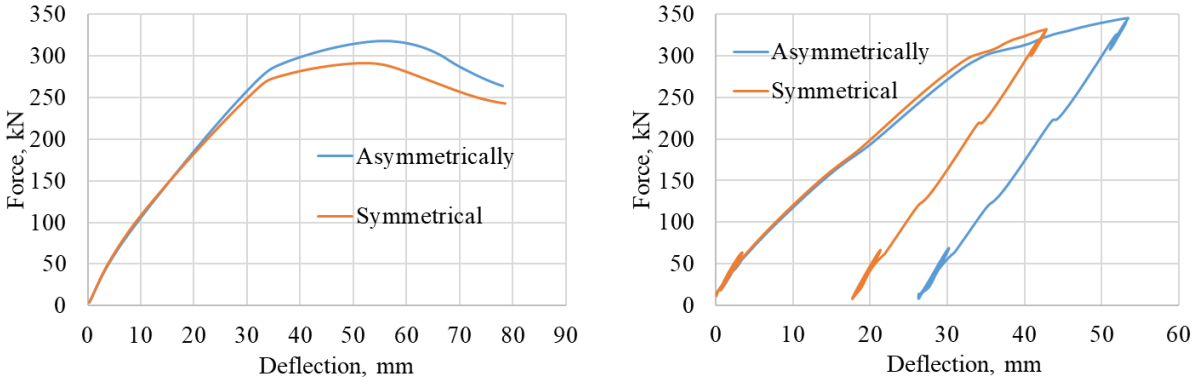

Figure 10. Time change in deflection (a) and load (b); N-f dependence under static (c) and dynamic (d) loading.

Fig. 11 shows the value of stresses arising in concrete and stiff rebars in the middle of the slab span for a standard cross-section under maximum dynamic loading. For nonsymmetrical loading, stress is 1.28 times the cylinder strength, which can be interpreted as the onset of concrete fracture in the top zone of the slab. For symmetrical loading, stresses do not exceed the cylinder strength. However for symmetrical loading, the bottom part of both stiff rebars, capable of resisting loads, is subjected to great plastic deformations, and is in the hardening zone with a bearing capacity margin of 13 % at the maximum resistance of 390 MPa. In case of nonsymmetrical loading, the behavior of the left stiff rod is elastic, while the right one has a 12 % safety margin for the maximum resistance. It confirms that dynamic nonsymmetrical loading is particularly dangerous in terms of the ultimate limit state of the structure. In addition to standard stresses, used for the preliminary evaluation of the stressed state of concrete and rebars, von Mises equivalent stresses in stiff rebars were computed, and the same about principal stresses $\sigma_1 - \sigma_3$ in concrete. The stress state of slab elements is the same as when only standard stresses are analyzed.

When the time change in standard stresses was analyzed according to Fig. 7a, the following characteristic states were considered:

- load in the course of normal operation (t = 0.5 c);
- an increase in dynamic loading up to the peak value (t = 0.7 c);
- maximum dynamic load (t = 1.2 c);
- the de-loading moment: the onset of vibrations together with the impactor (t = 1.4 c).

The distribution of stresses in the structure, corresponding to these moments in time, is shown in Fig. 12. The analysis of the figure shows that stresses in concrete do not stabilize at the moments of onset and termination of the peak dynamic load; on the contrary, they rise.

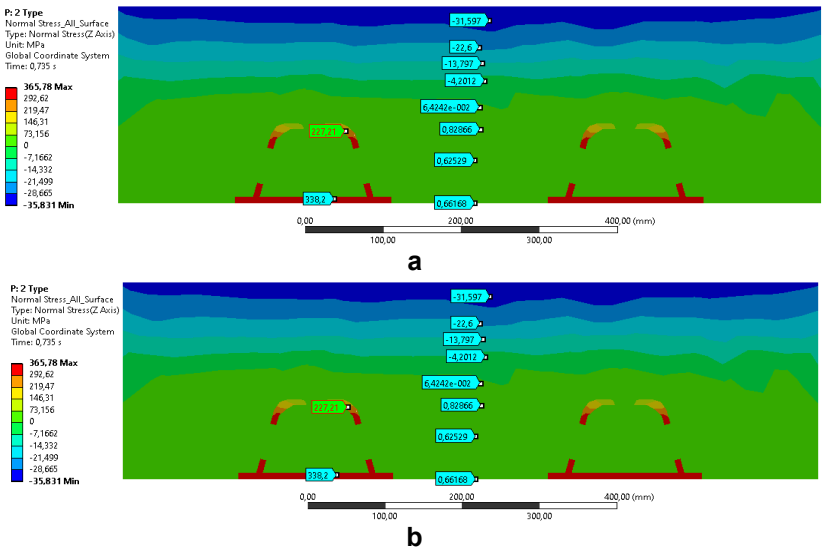

Figure 11. Stresses in the slab cross-section under symmetrical (a) and nonsymmetrical loading (b).

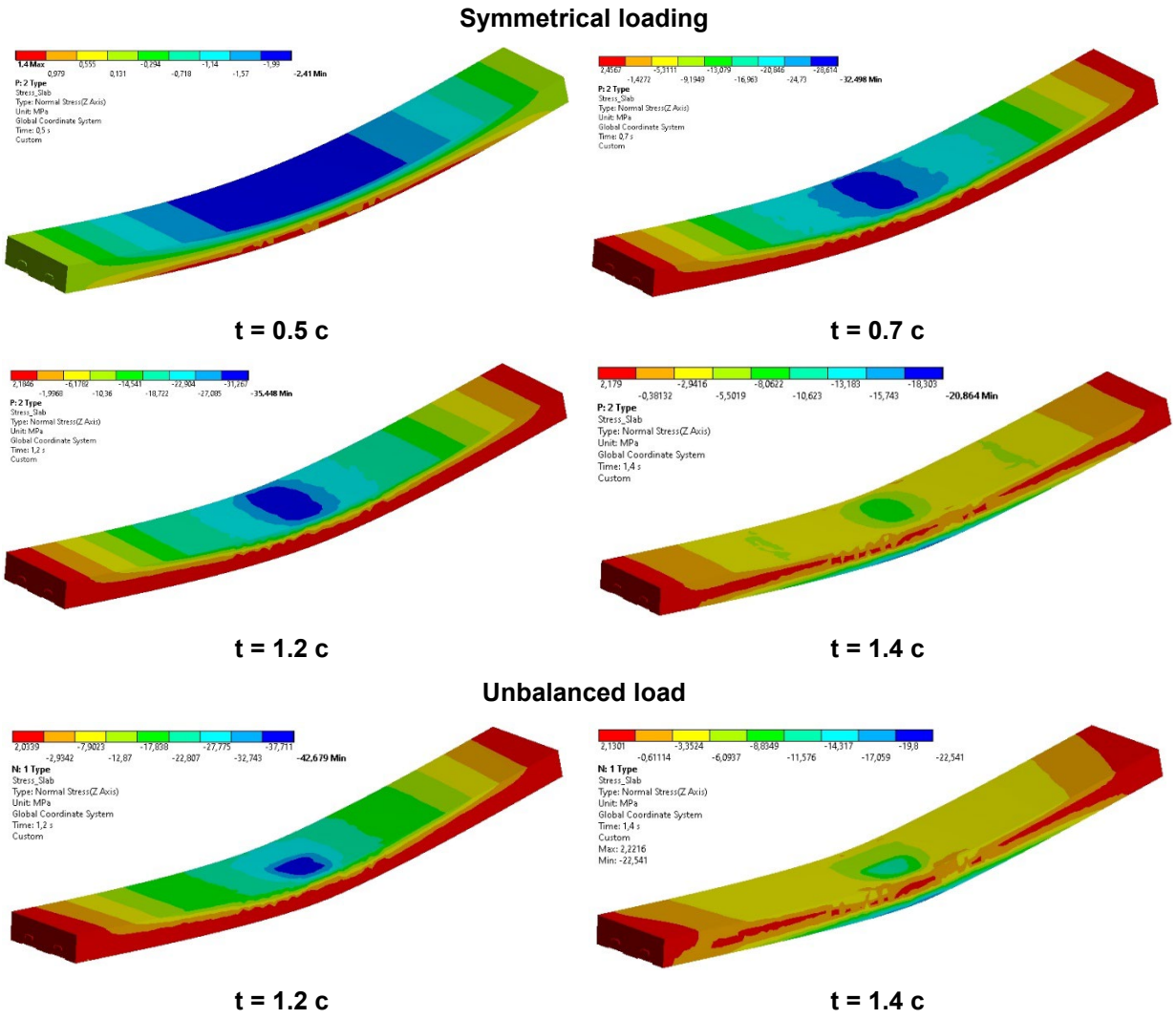

Figure 12. Time change in stresses in the slab concrete.

This indicates the importance of taking into account the time of application of peak dynamic load: if applied for a period longer than 1.2 – 0.7 = 0.5 s, it may lead to the collapse of the structure. In addition, at the moment of de-loading, tensile stresses, essential for cracking, emerge in the middle of the slab. The bottom zone of the slab is compressed. As a result of the further analysis of joint vibrations, the concrete tensile zone extends to the top part of the slab in the neighborhood of the area of dynamic load application. Hence, a conclusion can be made that the collapse of this structure predominantly follows the concrete fracture pattern.

3.1. Discussion

The use of stiff rebars in bending reinforced concrete elements nearly prevents the complete emergency collapse of structures, meaning that an increase in structural survivability can be discussed. This property was verified by making additional computations of pre-set displacements under static loading. Following the loss of bond with concrete in the bottom zone, the behavior of stiff slab rebars becomes similar to that of a beam, and later it behaves as a cable-stayed mechanism. In this case, its bearing capacity is determined by the bearing capacity of the profile of stiff rebars. Indeed, the slab preserved its bearing capacity, even when it was loaded by pre-set displacements up to 30 cm. Local rules and regulations have a deflection-based criterion of survivability; it equals 1/30 of the span. In the case under consideration, 600/30 = 20 cm, but when the loading of the structure triggered a deflection of 30 cm, the load-bearing capacity of stiff rebars was far from exhaustion. This allows us to suggest expanding and clarifying the survivability criteria for structures with stiff rebars.

The initial value of the dynamic load, needed to identify its limit value, was taken as 90 % of the static load value, but according to the computation results, the maximum value exceeded the static value by 8,5 % under nonsymmetrical loading and by 14 % under symmetrical loading, which may be due to inertial effects and hardening of materials.

The conducted research has promising prospects for comparing the accuracy of concrete models in the simulation of bridge structures. For instance, instead of the model used in [39], the models described in [37, 38] could be applied. Of particular interest is the simulation of the bond between concrete and rigid reinforcement. For this, the assumptions from the review [36] could be used, with the criterion in this work being evaluated based on the cohesion stress in the area of the stiff rebars. Since the surface area of the profile in contact with the concrete is large, no loss of bond between the concrete and reinforcement was observed in the calculations considered. Future studies will explore other profile shapes described in the article [40].

4. Conclusion

1. A numerical modeling method is proposed to simulate the stress-strain state of slabs of pedestrian bridges with stiff rebars. This method encompasses the use of experimentally verified 3D finite element schemes that allow taking into account the actual behavior of these structures.
2. It is identified that nonsymmetrical emergency effects are most dangerous for slabs and lead to structural concrete failure in the area of dynamic loading.
3. Stiff rebars are proven to be highly efficient for the bending elements considered in this article. It is found that stiff rebars prevent the complete fracture of a structure; they can rise the structural resistance to mechanical damage and the general level of mechanical safety of structures.
4. The survivability margin of these reinforced concrete slabs with stiff rebars is up to 50 % in terms of deflection constraints regulated by domestic and foreign standards.

References

1. Mahmoud, K.A. Lateral Deformation Behavior of Eccentrically Loaded Slender RC Columns with Different Levels of Rotational End Restraint at Elevated Temperatures. Journal of Structural Fire Engineering. 2021. 12(1). Pp. 35–64. DOI: 10.1108/JSFE-04-2020-0014
2. Kashani, M.M., Crewe, A.J., Alexander, N.A. Structural Capacity Assessment of Corroded RC Bridge Piers. Proceedings of the Institution of Civil Engineers: Bridge Engineering. 2017. 170(1). Pp. 28–41. DOI: 10.1680/jbren.15.00023
3. Yilmaz, T., Kiraç, N., Anil, Ö. Experimental Investigation of Axially Loaded Reinforced Concrete Square Column Subjected to Lateral Low-Velocity Impact Loading. Structural Concrete. 2019. 20(4). Pp. 1358–1378. DOI: 10.1002/suco.201800276
4. Isaac, O.S., Jagadeesh, G. Impulse Loading of Plates Using a Diverging Shock Tube. Experimental Mechanics. 2020. 60. Pp. 565–569. DOI: 10.1007/s11340-019-00573-5
5. Mai, V.C., Vu, N.Q., Nguyen, V.T., Pham, H. Ultra-High Performance Fiber Reinforced Concrete Panel Subjected to Severe Blast Loading. Defence Science Journal. 2020. 70(60). 603–611. DOI: 10.14429/DSJ.70.15835
6. Alekseytsev, A.V., Sazonova, S.A. Numerical Analysis of the Buried Fiber Concrete Slabs Dynamics under Blast Loads. Magazine of Civil Engineering. 2023. 117(1). Article no. 11703. DOI: 10.34910/MCE.117.3
7. Bregoli, G., Vasdravellis, G., Karavasilis, T.L., Cotsovos, D.M. Static and Dynamic Tests on Steel Joints Equipped with Novel Structural Details for Progressive Collapse Mitigation. Engineering Structures. 2021. 232. Article no. 111829. DOI: 10.1016/J.ENGSTRUCT.2020.111829
8. Li, Z.X., Zhang, X., Shi, Y., Wu, C., Li, J. Finite Element Modeling of FRP Retrofitted RC Column against Blast Loading. Compos Struct 2021. 263. Article no. 113727. DOI: 10.1016/j.compstruct.2021.113727
9. Mishra, N., Netula, O. Behaviour of Reinforced Concrete Framed Structure Subjected to Blast Loading. International Journal of Advanced Research in Engineering and Technology (IJARET). 2021. 12(1). 173–181. DOI: 10.34218/IJARET.12.1.2021.014
10. Zhou, X., Jing, L. Deflection Analysis of Clamped Square Sandwich Panels with Layered-Gradient Foam Cores under Blast Loading. Thin-Walled Structures. 2020. 157. Article no. 107141. DOI: 10.1016/j.tws.2020.107141
11. Siguerdjidjene, H., Dyachenko, L.K. Study of Dynamic Impact of Speed Trains on Bridge Structures. International Journal of Mechanics. 2021. 15. Pp. 30–36. DOI: 10.46300/9104.2021.15.4
12. Zhao, W., Qian, J., Wang, J. Performance of Bridge Structures under Heavy Goods Vehicle Impact. Computers and Concrete. 2018. 22(6). 515–525. DOI: 10.12989/cac.2018.22.6.515
13. Fan, W., Shen, D., Huang, X., Sun, Y. Reinforced Concrete Bridge Structures under Barge Impacts: FE Modeling, Dynamic Behaviors, and UHPFRC-Based Strengthening. Ocean Engineering 2020. 216. Article no. 108116. DOI: 10.1016/j.oceaneng.2020.108116
14. Fu, T., Zhu, Z., Li, Y., Sun, Y., Meng, L. Study on the Time-Dependent Reliability of Corroded Reinforced Concrete Bridge Structures Due to Ship Impact. Advances in Civil Engineering. 2022. 2022. Article no. 8190297. DOI: 10.1155/2022/8190297
15. Zhang, J., Wang, R., Han, W., Bao, H. A Comprehensive Approach for Bridge Performance Evaluation under Rockfall Impact Integrated with Geological Hazard Analysis. Engineering Failure Analysis. 2022. 141. Article no. 106668. DOI: 10.1016/j.engfailanal.2022.106668
16. Liu, Z., Lu, Z., Li, Y., Hu, R., Tu, B. Study on Impact Resistance of Flexible Shed Tunnel for Bridges in Mountainous Areas. Tiedao Xuebao/Journal of the China Railway Society. 2023. 45. DOI: 10.3969/j.issn.1001-8360.2023.03.015
17. Terrenzi, M., Spacone, E., Camata, G. Collapse limit state definition for seismic assessment of code-conforming RC buildings. 2018. International Journal of Advanced Structural Engineering. 10(3). Pp. 325–337. DOI: 10.1007/s40091-018-0200-6
18. Sinković, N.L., Dolšek, M. Fatality risk and its application to the seismic performance assessment of a building. Engineering Structures. 2020. 205. Article no. 110108. DOI: 10.1016/j.engstruct.2019.110108
19. Shokrabadi, M., Burton, H.V. Risk-based assessment of aftershock and mainshock-aftershock seismic performance of reinforced concrete frames. Structural Safety. 2018. 73. Pp. 64–74. DOI: 10.1016/j.strusafe.2018.03.003
20. Sinković, N.L., Brozovič, M., Dolšek, M. Risk-based seismic design for collapse safety. Earthquake Engineering and Structural Dynamics. 2016. 45(9). Pp. 1451–1471. DOI: 10.1002/eqe.2717

21. Thai, D.K., Pham, T.H., Nguyen, D.L. Damage assessment of reinforced concrete columns retrofitted by steel jacket under blast loading. Structural Design of Tall and Special Buildings. 2020. 29(1). Article no. e1676. DOI: 10.1002/tal.1676
22. Alekseytsev, A.V. Mechanical safety of reinforced concrete frames under complex emergency actions. Magazine of Civil Engineering. 2021. 103(3). Article no. 10306. DOI: 10.34910/MCE.103.6
23. Kristoffersen, M., Hauge, K.O., Minoretti, A., Børvik, T. Experimental and numerical studies of tubular concrete structures subjected to blast loading. Engineering Structures. 2021. 233. Article no. 111543. DOI: 10.1016/j.engstruct.2020.111543
24. Maazoun, A., Matthys, S., Belkassem, B., Atoui, O., Lecompte, D. Experimental study of the bond interaction between CFRP and concrete under blast loading. Composite Structures. 2021. 277. Article no. 114608. DOI: 10.1016/j.compstruct.2021.114608
25. Li, Z.X., Zhang, X., Shi, Y., Wu, C., Li, J. Finite element modeling of FRP retrofitted RC column against blast loading. Composite Structures. 2021. 263. Article no. 113727. DOI: 10.1016/j.compstruct.2021.113727
26. Alekseytsev, A.V., Gaile, L., Drukis, P. Optimization of steel beam structures for frame buildings subject to their safety requirements. Magazine of Civil Engineering. 2019. 91(7). Pp. 3–15. DOI: 10.18720/MCE.91.1
27. Kumpyak, O.G., Galyautdinov, Z.R., Kokorin, D.N. AIP Conference Proceedings. 2016. 1698(1). Article no. 070006. DOI: 10.1063/1.4937876
28. Chen, Y., May, I.M. Reinforced concrete members under drop-weight impacts. 2009. Proceedings of the Institution of Civil Engineers: Structures and Buildings. 162(1). Pp. 45–56. DOI: 10.1680/stbu.2009.162.1.45
29. Qasrawi, Y., Heffernan, P.J., Fam, A. Dynamic behaviour of concrete filled FRP tubes subjected to impact loading. Engineering Structures. 2015. 100. Pp. 212–225. DOI: 10.1016/j.engstruct.2015.06.012
30. Ngo, T., Mendis, P. Modelling the dynamic response and failure modes of reinforced concrete structures subjected to blast and impact loading. Structural Engineering and Mechanics. 2009. 32(2). Pp. 269–282. DOI: 10.12989/sem.2009.32.2.269
31. Niroomandi, A., Pampanin, S., Dhakal, R.P., Ashtiani, M.S., De La Torre, C. Rectangular RC walls under bi-directional loading: recent experimental and numerical findings. The Concrete NZ Conference 2018. Hamilton, 2018.
32. Magnusson, J., Hallgren, M., Ansell, A. Shear in concrete structures subjected to dynamic loads. Structural Concrete. 2014. 15(1). Pp. 55–65. DOI: 10.1002/suco.201300040
33. Alekseytsev, A.V. Stability of the RC Column under Horizontal Impacts. Reinforced concrete structures. 2023. 2(2). Pp. 3–12. DOI: 10.22227/2949-1622.2023.2.3-12
34. ANSYS Mechanical APDL Verification Manual. https://www.researchgate.net/profile/Girish-Prajapati-2/post/How-composites-can-be-modeled-in-ANSYS-Using-Solid185/attachment/59d6250379197b8077983549/AS%3A315291291062272%401452182710434/download/ANSYS+Mechanical+APDL+Verification+Manual.pdf
35. Dmitriev, A., Novozhilov, Y., Mikhalyuk, D., Lalin, V. Calibration and Validation of the Menetrey-Willam Constitutive Model for Concrete. Construction of Unique Buildings and Structures. 2020. 88. Article no. 8804. Pp. 84–91. DOI: 10.18720/CUBS.88.4
36. Korsun, V.I., Karpenko, S.N., Makarenko, S.Yu., Nedoresov, A.V. Modern strength criteria for concrete under triaxial stress states. Building and Reconstruction. 2021. 97(5). Pp. 16–30. DOI: 10.33979/2073-7416-2021-97-5-16-30
37. Budarin, A.M., Rempel, G.I., Kamzolkyn, A.A., Alekhin, V.N. Stress-strain concrete model with double independent reinforcement. Vestnik MGSU [Monthly Journal on Construction and Architecture]. 2023. 18(4). Pp. 517–532. DOI: 10.22227/1997-0935.2023.4.517-532
38. fib Model Code for Concrete Structures 2010. International Federation for Structural Concrete, 2013. 434 p. DOI: 10.1002/9783433604090
39. Menétrey, Ph. Numerical analysis of punching failure in reinforced concrete structures. PhD thesis. L'école polytechnique fédérale de Lausanne. Lausanne, 1994. p. 179.
40. Al Ali, M., Kvočák, V., Dubecký, D., Alekseytsev, A. Experimental research on composite deck bridges with encased steel beams. Delta University Scientific Journal. 2023. 6(1). Pp. 31–38. DOI: 10.21608/dusj.2023.291004
41. Alekhin, V., Budarin, A., Pletnev, M., Avdonina, L. MATEC Web of Conferences. 2019. 279(2). Article no. 02005. DOI: 10.1051/matecconf/201927902005
42. Turteltaub, S. Inelastic analysis of structures, Milan Jirásek and Zdeněk P. Bažant, John Wiley & Sons, 2002, ISBN 0-471-98716-6, 758 Pages. Structural and Multidisciplinary Optimization. 2002. 24. Pp. 87–88. DOI: 10.1007/s00158-002-0217-z

Information about the authors:

***Anatoly Alekseytsev**, Doctor of Technical Sciences*
ORCID: https://orcid.org/0000-0002-4765-5819
E-mail: aalexw@mail.ru

***Vincent Kvocak**, Doctor of Engineering*
ORCID: https://orcid.org/0000-0002-5229-638X
E-mail: vincent.kvocak@tuke.sk

***Dmitry Popov**, PhD in Technical Sciences*
ORCID: https://orcid.org/0000-0003-0768-8808
E-mail: popovds89@mail.ru

***Mohamad Al Ali**, PhD in Technical Sciences*
E-mail: mohamad.alali@tuke.sk

Received 29.07.2024. Approved after reviewing 05.01.2025. Accepted 12.01.2025.